water

MDPI

Article

Degradation of Azo Dyes with Different Functional Groups in Simulated Wastewater by Electrocoagulation

Yang Liu [1,*], Chenglong Li [1], Jia Bao [1,*], Xin Wang [1], Wenjing Yu [2] and Lixin Shao [1]

[1] School of Environmental and Chemical Engineering, Shenyang University of Technology, Shenyang 110870, China; lichenglong@sut.edu.cn (C.L.); xinwang@sut.edu.cn (X.W.); shaolx@sut.edu.cn (L.S.)
[2] School of Water Resources & Environment, China University of Geosciences, Beijing 100083, China; yuwenjing@sut.edu.cn
* Correspondence: liuyang@sut.edu.cn (Y.L.); baojia@sut.edu.cn (J.B.)

Abstract: Increasing attention has been paid to the widespread contamination of azo dyes in water bodies globally. These chemicals can present high toxicity, possibly causing severe irritation of the respiratory tract and even carcinogenic effects. The present study focuses on the periodically reverse electrocoagulation (PREC) treatment of two typical azo dyes with different functional groups, involving methyl orange (MO) and alizarin yellow (AY), using Fe-Fe electrodes. Based upon the comparative analysis of three main parameters, including current intensity, pH, and electrolyte, the optimal color removal rates for MO and AY could be achieved at a rate of up to 98.7% and 98.6%, respectively, when the current intensity is set to 0.6 A, the pH is set at 6.0, and the electrolyte is selected as NaCl. An accurate predicted method of response surface methodology (RSM) was established to optimize the PREC process involving the three parameters above. The reaction time was the main influence for both azo dyes, while the condition of PREC treatment for AY simulated wastewater was time-saving and energy conserving. According to the further UV–Vis spectrophotometry analysis throughout the procedure of the PREC process, the removal efficiency for AY was better than that of MO, potentially because hydroxyl groups might donate electrons to iron flocs or electrolyze out hydroxyl free radicals. The present study revealed that the functional groups might pose a vital influence on the removal efficiencies of the PREC treatment for those two azo dyes.

Keywords: azo dyes; functional groups; chemical oxygen demand (COD); color removal; response surface methodology (RSM); periodically reverse electrocoagulation (PREC)

Citation: Liu, Y.; Li, C.; Bao, J.; Wang, X.; Yu, W.; Shao, L. Degradation of Azo Dyes with Different Functional Groups in Simulated Wastewater by Electrocoagulation. *Water* **2022**, *14*, 123. https://doi.org/10.3390/w14010123

Academic Editor: Alexandre T. Paulino

Received: 20 October 2021
Accepted: 3 January 2022
Published: 5 January 2022

1. Introduction

The environmental problems originating from the textile industry have been receiving increasing attentions for several decades, since the textile industry is one of the major sources of contaminated effluents [1]. Azo dyes are the most widely used dyes and comprise over 60% of the total dyes used [2]; these dyes include compounds consisting of a diazotized amine coupled to an amine or a phenol, as well as containing one or more azo linkages. According to the statistical data reported previously, azo dyes account for over 80% of the total dyes produced globally each year, and they have been widely used in the textile and dyeing, papermaking, printing, leather, cosmetics and pharmaceutical industries [3]. Presumably, around 2000 types of azo dyes are currently used, and more than 70,000 tons of these dyes are manufactured worldwide annually [4]. For example, the textile water consumption values in the tops/fiber and yarn production vary between 35 and 180 L per kg^{-1} of product. Moreover, the water consumption values in the yarn mills range between 43 and 212 L per kg^{-1} of product, and those in the fabric finishing mills were in the range of 60 and 216 L per kg^{-1} of product [5].

Azo dyes can have negative impacts on the water quality of both surface water and groundwater, such as blocking light transmission, affecting photosynthesis of plants and

algae in water, and reducing dissolved oxygen in water [6]. Furthermore, azo dyes could be accumulated in the aquatic systems, possibly causing carcinogenicity and mutagenicity to various species of fishes [7,8]. Azo dyes can transport along both aquatic and terrestrial pathways, thus entering the food chain and then posing health risks to organisms and humans [9]. Moreover, azo dye wastewaters have several adverse impacts on the aquatic environment in terms of the total organic carbon (TOC), biochemical oxygen demand (BOD), chemical oxygen demand (COD), suspended solids (SS), salinity, color, and a wide range of pH (5–12). Normally, the ratio of BOD/COD for azo dye wastewaters ranges from 0.2 to 0.5, indicating that these effluents contain a large proportion of non-biodegradable organic matter [2]. The presence of azo dyes in surface and subsurface water might make the aquatic organisms intolerable, and may even lead to many diseases of mucous membranes in the human body, e.g., dermatitis, perforation of the nasal septum, and severe irritation of the respiratory tract [10]. Therefore, the treatment of azo dye wastewaters has become an important environmental concern [11].

Azo dyes are characterized by the variety in chemical structures, resulting in environmental stability against heat and ultraviolet light and resistance to microbial degradation or discoloration. For instance, azo dyes usually contain a strong stable benzene ring structure, and even dissolved functional groups of sulfonate, hydroxyl, or carboxyl, leading to difficulty in carrying out water treatment. Some modern technologies have been applied to mitigate the degradation of azo dyes, such as electrochemical methods, ozone oxidation, photo Fenton, chemical precipitation, membrane separation, adsorption, and photocatalysis [12–14]. However, the material regeneration performance of adsorption technology would be inefficient, and membrane separation technology might be restricted by membrane pollution and unstable membrane flux, while other technologies require strict operating conditions, such as high material cost, long processing time, or high energy consumption [15,16]. Recent studies have demonstrated that electrochemical methods have been widely employed in the degradation of organic pollutants in various wastewaters, because of high removal efficiency and low energy consumption [17]. Electrochemical methods comprise electrocoagulation (EC), electrocatalytic oxidation [18], bioelectrochemistry [19], and electroreduction [20]. Among them, the EC method has the advantage of strong applicability, a high degree of automation, high efficiency, and low cost, and thus could be an attractive treatment technique for dye wastewaters.

The EC process involves the dissolution of charged cations (e.g., Zn^{2+}, Al^{3+}, Fe^{3+}) originated from the sacrificial anode, forming monomeric and polymeric hydroxyl complex species simultaneously, which can strongly sorb certain pollutants from contaminated water [21]. For instance, 95.3% of brilliant green dye and 98% of reactive red 120 dye from drinking water could be removed by the EC process [22,23]. Nunez et al. used the EC technique for the dye degradation in wastewater in a batch-stirred EC reactor with iron and aluminum as anode materials simultaneously, and subsequently the removal efficiency of color and COD achieved was 86% and 59%, respectively [24].

Compared with the conventional EC technique, the periodically reverse electrocoagulation (PREC) technique could remove unmanageable perfluoroalkyl substances (PFASs) swiftly and efficiently, and avoid passivation on the electrode surface in the practical applications [25–27]. So far, researchers have always focused on the EC efficiency for azo dyes, however, different functional groups of azo dyes results in EC treatment having various degrees of efficiency. For instance, the optimum color removal efficiency of indigo carmine (IC) was 72% by the EC technique [28], while the color removal rate of reactive red 120 was 93.47% [29]. Therefore, further studies would be warranted to focus on the operating conditions, removal efficiencies, and degradation mechanisms of the PREC technique for the treatment of typical azo dyes with different functional groups in various wastewaters.

In the present study, the PREC technique was applied to achieve the following objectives: (1) comparing the treatment efficiency of PREC for the simulated aqueous solution containing either methyl orange (MO) or alizarin yellow (AY) with single-factor involving current intensity, pH, and electrolyte; (2) establishing a reliable model of response surface

methodology (RSM) to investigate the main effects of multiple factors and determine the optimal PREC process to remove azo dyes; and (3) reveal the degradation mechanism via further spectrophotometry analysis on diverse functional groups of MO and AY.

2. Materials and Methods

2.1. Chemicals and Reagents

Methyl orange (99.9%) and alizarin yellow (99.9%) were acquired from Fluka (Steinheim, Germany). HPLC grade of sodium chloride (NaCl), hydrochloric acid (HCl), sodium carbonate (Na_2CO_3), sodium sulfate (Na_2SO_4), and ethanol (C_2H_6O) were purchased from Acros Organics (Geel, Belgium). All solutions were prepared using ultrapure water with a conductance of 18.2 MΩ cm^{-1} (Millipore, Bedford, MA, USA).

2.2. Experimental Setup and Procedure

The reactor for degradation of MO and AY in simulated wastewater was an organic glass electrolytic cell with an effective volume of 400 mL with two parallel metal electrodes, and the individual size of the electrode was 5 cm × 4 cm × 0.2 cm. The electrodes were immersed vertically in simulated wastewater of MO or AY completely, and stirred continuously using a magnetic stirrer (IKARCT, Germany). The electrodes were connected to a digital DC power supply, characterized by the ranges of 0-3 A for current intensity and 0–30 V for voltage.

Mutual combinations by Fe-Fe electrodes were adopted for the PREC treatment of MO or AY wastewater, since iron is one of the most common elements in nature and fresh waters [30]. Contaminants could be oxidatively degraded, floated, enmeshed, or adsorbed by the metal hydroxide flocs generated in-situ by electro-oxidation, in turn as the sacrificial anode [26], while the passivation coating was eliminated as the cathode mode. In this study, iron was selected as the bipolar plate material. The plates were fully submerged into the solution in the reactor during all experiments, and were cleaned manually before each run by abrasion with sand paper and treatment with 15% hydrochloric acid, followed by washing with distilled water [27]. Based upon the important influence parameters mentioned earlier [31–33], the current intensity in the range between 0.4 and 0.8 A, pH between 3.0 and 9.0, and three electrolytes of Na_2SO_4, Na_2CO_3, and NaCl with 2 g L^{-1} was selected for the optimal single-factor impact experimental design. In addition, the initial concentrations of both MO and AY in the simulated aqueous solution were set to 100 mg L^{-1}, the gap between two electrodes was fixed at 2 cm, stirring speed was 1000 r min^{-1}, and the reversing time was 10 s. An amount of 2 mL of simulated aqueous solution was sampled with an interval of 10 min and then filtered with 0.22 mm membrane (glass fiber filter) for the additional analysis of MO and AY concentration. Experiments were performed at the ambient temperature.

2.3. Sample Preparation and Analysis

The experiment duration of each PREC process was 50 min. Samples were taken every ten minutes. The reactor effluent from MO and AY wastewater treatment was analyzed after filtration through a glass fiber membrane. The wavelength of the sample was scanned using an ultraviolet and visible (UV–Vis) spectrophotometer (DR 5000, Hach Company, Loveland, CO, USA) [34]. Subsequently, the absorbances were determined to calculate the color removal of MO and AY with the maximum absorption wavelengths of 462 nm and 372 nm and the standard curves for MO ($y = 0.059x + 0.0015$, $R^2 = 0.996$) and AY ($y = 0.023x + 0.0026$, $R^2 = 0.999$), respectively. After digestion of each sample, the COD was analyzed by the COD detector (ET 99718, Lovibond, Germany). An amount of 1.0 M of H_2SO_4 and NaOH individually were used to adjust the desired pH [34].

2.4. Data Analysis

1. Color Removal (η) %

$$\eta = \frac{A_0 - A_t}{A_0} \%$$

A_0 and A_t are the absorbances of MO and AY in wastewater at the corresponding wave length (λmax) before and after the treatment.

2. COD Removal (δ) %

$$\delta = \frac{[(COD) - (COD_t)]}{COD} \%$$

COD and COD_t are the chemical oxygen demand of MO and AY in wastewater before and after the treatment.

2.5. RSM Experimental Design

Design Expert V8.0.6.1 statistical software was used to carry out the experimental design, analysis of variance (ANOVA), mathematical modelling, and 3D response surface. Three important operating parameters involving the current intensity (A), time (min) and pH were studied and optimized using the Box–Benkhen Experimental Design (BBD) at three levels when the electrolyte was selected as NaCl. The experimental factors and levels are shown in Table 1. The statistical significance of the produced models was evaluated through ANOVA. Residual plots and coefficients of determination (R^2, Adjusted R^2, and Predicted R^2) were presented to express the quality of the fitted models [31,32].

Table 1. Response surface test factor level table.

Parameter	Horizontal Extent		
	−1	**0**	**1**
Current intensity (A)	0.4	0.6	0.8
Time (min)	10	30	50
pH	3	6	9

3. Results and Discussion

3.1. The Influence of Current Intensity

Current intensity is commonly considered as an important factor for removing pollutants effectively in the PREC process. The current intensity determines the amount of sacrifice electrodes dissolution, which affects the generation of metal hydroxide flocs, as well as the removal efficiency of contaminants consequently [35]. The influence of current intensity in the range between 0.4 and 0.8 A on MO or AY wastewater was investigated in this study, with the conditions of 2 g L^{-1} NaCl and pH at 6.0. The color removal rates of MO and AY influenced by different current intensity are shown in Figure 1a. The color removal rates of MO and AY altogether increased with the current intensity, and the removal rates of MO and AY were up to 90.7% and 95.0% at 20 min, respectively, when the current intensity was set at 0.6 A. This verified that MO and AY tended to be removed by the adsorption of generation flocs [36]. Meanwhile, the higher removal rate of AY might result in more electron-donating groups involving -OH in AY that facilitate adsorption on flocs. According to the Faraday's law, the amount of sacrifice electrodes dissolution and OH^- concentration were positively correlated with the current intensity, leading to additional hydroxide flocs formation that facilitate MO and AY adsorption. However, when the current intensity was set at 0.8 A, an increase in the current intensity beyond the optimal value had little effect on the contaminant removal efficiency, as reported previously [37]. Because the extra current intensity would increase superfluous small size bubbles that resist aggregate formation for contamination adsorption [27]. In addition, extra current intensity would generate higher energy consumption and steady color removal. Therefore, the optimal current intensity for removing the colors of MO and AY in wastewater was determined as 0.6 A.

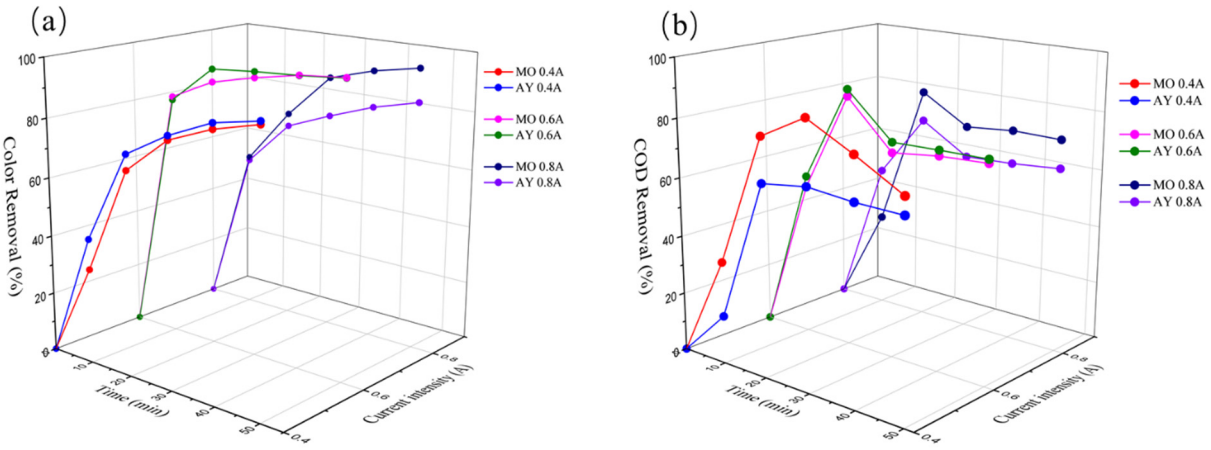

Figure 1. The effect on color and COD removal of MO (**a**) and AY (**b**) in wastewater with different current intensity.

As shown in Figure 1b, when the current intensity was set at 0.6 A, the optimum COD removal rates for MO and AY could reach 86.2% and 88.6% at 20 min individually. The COD removal rates increased with the current intensity within the first 20 min due to the complete adsorption of contamination onto the flocs. However, the COD removal rates appearing to display a decreasing trend subsequently remained relatively stable over time. On one side, dissolved ferrous iron could be oxidized by the COD agent in the PREC process [38]. On the other side, active free radicals, such as ·OH and $O_2 \cdot^-$, could be generated by catalyzing O_2 and Fe^{2+} during the PREC process [39], thus oxidative degradation occurred during the subsequent reaction process, generating hardly degradable by-products containing a benzene ring structure. Therefore, the COD removal could be achieved quickly in the initial stage, while further oxidative degradation needed to be enhanced after then.

3.2. The Influence of pH

The pH of the aqueous solution is regarded as another factor for removing contaminants effectively during the electrocoagulation process [40,41], which could influence the dissolution of electrodes, as well as the structure and morphology of hydroxide flocs generated from the dissolved anode, thus affecting the contamination removal efficiency [15]. In the PREC process, Fe was oxidized at the anode ($Fe \rightarrow Fe^{2+} + 2e^-$, $Fe^{2+} \rightarrow Fe^{3+} + e^-$, $Fe \rightarrow Fe^{3+} + 3e^-$), while reduction reaction was produced at the cathode ($2H_2O + 2e^- \rightarrow 2OH^- + H_2$). Therefore, iron hydroxide complexes were formed in the solution, and the surface charge of the electrocoagulation flocs also varied with the growth of pH during electrolysis. In the present study, the influences of pH values with 3.0, 6.0, and 9.0 on the removal efficiencies of MO and AY in the simulated wastewater were estimated separately, with the conditions of 2 g L^{-1} NaCl and current intensity at 0.6 A. As shown in Figure 2a, the color removal efficiencies of MO and AY increased rapidly in the initial 20 min, and improved progressively during the next reaction process. Moreover, solutions with a neutral pH at 6.0 were more favorable than the acidic and alkaline solutions for the degradation of MO and AY by the PREC treatment, and the color removal efficiencies for MO and AY were up to 98.7% and 98.6%, respectively. In the acidic environment, the iron electrode was inclined to be dissolved, with the form of Fe^{2+} or Fe^{3+} in the aqueous solution. In the alkaline environment, the sediment of $Fe(OH)_3$ and $Fe(OH)_2$ could develop a passivating surface layer at the electrode, because their solubility limits were exceeded [42]. Based upon the predominance-zone diagram for Fe(II) and Fe (III) species in the aqueous solution in the function of pH [43], in the neutral solution of pH at 6.0, the precipitation of $Fe(OH)_2$ and $Fe(OH)_3$ were gradually generated in the solution to remove MO and AY contaminants mainly by the adsorption of enmeshment. Consequently, the optimum pH value for the elimination of MO and AY from aqueous solutions could be fixed at 6.0.

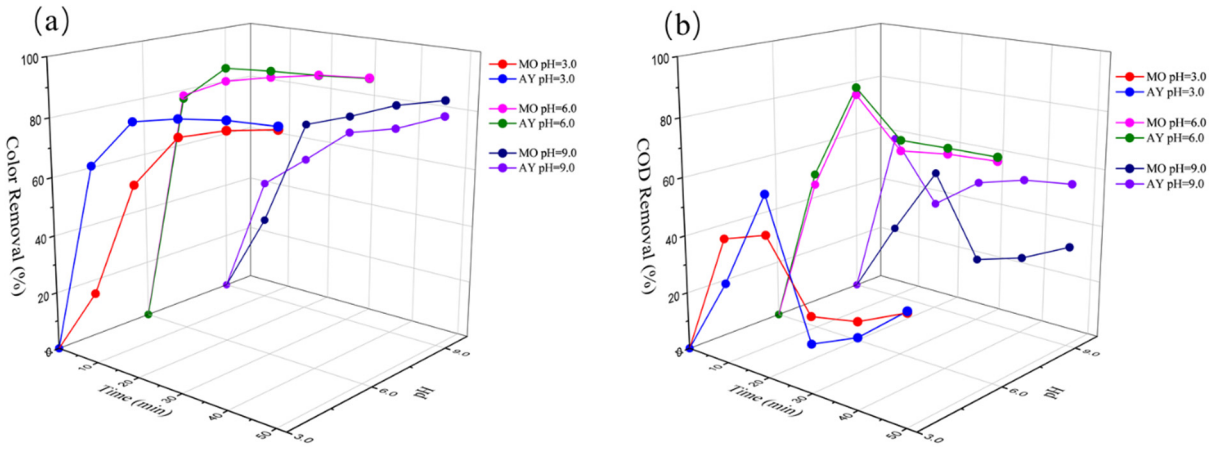

Figure 2. The effect on color and COD removal of MO (**a**) and AY (**b**) in wastewater with diverse pH.

As shown in Figure 2b, the COD removal of MO and AY increased in the initial 20 min, but decreased following this. This may be related to the strengthening adsorption in the initial stage, while the chemical structure was destroyed by ·OH and formed a benzene ring later [39]. In addition, when the pH values were 3.0, 6.0, and 9.0, the COD removal rates of MO at 20 min reached 48.0%, 86.2%, and 51.2%, respectively. Meanwhile, the COD removal rates of AY achieved 61.3%, 88.6%, and 39.8%, respectively. Therefore, the pH value of 6.0 was suitable for the elimination of MO and AY from aqueous solutions.

3.3. The Influence of Electrolyte

In the PREC process, the suitable supporting electrolyte in solution could avoid passivation of electrodes, increase the solution conductivity, accelerate the rate of proton migration, and diminish the ohmic drop and the energy consumption [44]. In the present study, the effects of three electrolytes (Na_2SO_4, Na_2CO_3, and NaCl) on the degradation of MO and AY by the PREC were investigated, with the current intensity at 0.6 A and pH at 6.0. As shown in Figure 3a,b, when the electrolyte was Na_2SO_4 or Na_2CO_3, the color and COD removal for either MO or AY were less effective. When the electrolyte was Na_2SO_4, Na_2CO_3 and NaCl, the color removal rates of MO at 20 min were 54.9%, 74.8%, and 90.7%, meanwhile, 75.3%, 60.4%, and 95.3% for AY, respectively. Correspondingly, the COD removal rates of MO at 20 min were 34.5%, 65.3%, and 86.2%, but 70.0%, 49.0%, and 88.6% for AY, respectively. Therefore, the electrolyte of NaCl was beneficial for the degradation of azo dyes, contributing to improved electrical conductivity of the solution using NaCl, thus increasing the overall removal efficiency. In addition, Cl^- could generate Cl_2 during the procedure of chlorine evolution reaction, and then hydrolysis reaction happened in the electrocoagulation system for the generation of HClO, which simultaneously strengthened the attack effect of the base groups in MO and AY and the oxidation of oxides [44]. On the other hand, the chloride medium significantly favored the PREC process, owing to large corrosive power of chlorides that could promote the release of coagulant species. In addition, the color and COD removal efficiency of AY were superior to the MO without the influence of electrolytes, which demonstrates that the chemical structure of AY is inclined to be treated by the PREC technique. Based upon the functional group of electron-donating group involving -OH of AY might easily result in electric attraction with Fe hydroxide flocs, or redox reaction in the solution [30]. This phenomenon requires further analysis in regard to the influence of functional groups. Therefore, NaCl can be considered as the optimal electrolyte applied in the PREC treatment of MO and AY in simulated wastewater.

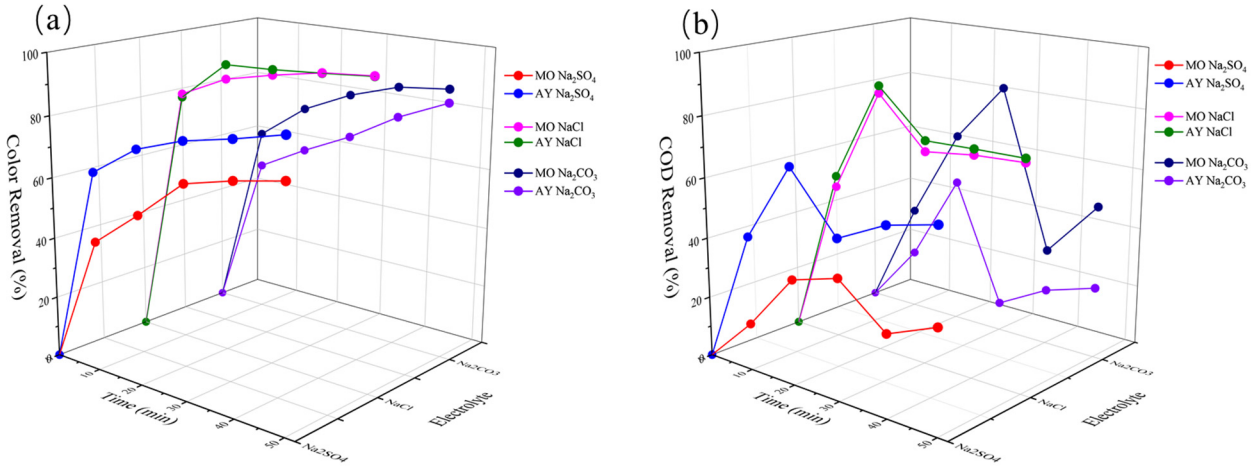

Figure 3. The effect on color and COD removal of MO (**a**) and AY (**b**) in wastewater with various electrolytes.

3.4. Analysis of RSM

RSM is an improved method that optimizes the process and operating variables at different levels [45]. In the present study, three significant influencing parameters are selected and optimized at three levels through ANOVA, mathematical modeling, and the color removal rates of MO and AY in the PREC process are the response value. The test results are listed in Table 2.

Table 2. Results of the experiment of MO and AY.

The Experiment Number	MO				AY			
	Current Intensity (A)	Time (min)	pH	Color Removal Rate	Current Intensity (A)	Time (min)	pH	Color Removal Rate
1	0.60	10.00	3.00	24.8	0.80	30.00	3.00	99.08
2	0.40	10.00	6.00	65.7	0.40	30.00	3.00	99.01
3	0.40	30.00	3.00	98.33	0.40	10.00	6.00	75.6
4	0.60	50.00	9.00	85.4	0.60	10.00	3.00	67.1
5	0.80	30.00	3.00	90.77	0.60	10.00	9.00	69
6	0.60	30.00	6.00	94.3	0.80	50.00	6.00	85
7	0.80	50.00	6.00	99.3	0.60	30.00	6.00	95
8	0.80	30.00	9.00	97.95	0.60	50.00	3.00	91.2
9	0.80	10.00	6.00	74.1	0.80	30.00	9.00	97.31
10	0.60	50.00	3.00	90.2	0.60	30.00	6.00	98.83
11	0.40	50.00	6.00	91	0.80	10.00	6.00	54
12	0.60	10.00	9.00	29.9	0.40	30.00	9.00	99.24
13	0.60	30.00	6.00	95.84	0.60	30.00	6.00	96.76
14	0.40	30.00	9.00	94.22	0.40	50.00	6.00	72
15	0.60	30.00	6.00	94.85	0.60	50.00	9.00	80.1

The significance of the model and its items were evaluated via the F-value and p-value by ANOVA. When the p-value was lower than 0.05, the test variables were significant. As shown in Table 3, the MO independent variables of time (B and B^2) and pH (C^2) were significant for the removal efficiency, however, the interaction of AB, AC, and BC were insignificant. According to the parameters of the *p*-value < 0.05 and R^2 = 0.9002 obtained from the table, it concluded that the prediction model was well developed. As shown in Table 4, AY independent variables of time (B and B^2) and pH (C^2) were significant, and the interaction of AB and BC was significant, while the interaction of AC were insignificant for the experiment. Therefore, the influence parameters for the azo dyes by the PREC followed the order of B > C > A, the interaction between current intensity and time as well as the interaction between time and pH were impactful for AY. The predicted R^2 = 0.8858 was

in reasonable agreement with the adjusted R^2 = 0.9742 because the difference was less than 0.2. The signal of noise ratio about Adeq Precision = 24.309 > 4, indicating that the signal was adequate due to being in the desirable region. According to the parameters of *p*-value < 0.0001 and R^2 = 0.9908, which concluded that the prediction model was well suitable for describing the PREC experimental data. In addition, as presented in Figure 4, all residuals spread along the straight line and exhibited the normal distribution of the obtained MO and AY removal rates. Furthermore, Figure 5 correspondingly showed the predicted values and actual values of removal rates as another confirmation.

Table 3. MO ANOVA results for response surface of quadratic model.

Source	Sum of Squares	df	Mean Square	F-Value	*p*-Value	
Model	6941.66	9	771.30			
A-Current intensity (A)	539.89	1	539.89	5.01	0.0454	significant
B-Time (min)	3672.24	1	3672.24	3.51	0.1200	
C-pH	20.42	1	20.42	23.85	0.0045	
AB	2.500E-003	1	2.500E-003	0.13	0.7306	
AC	0.88	1	0.88	1.624E-005	0.9969	
BC	24.50	1	24.50	5.739E-003	0.9426	
A^2	134.22	1	134.22	0.16	0.7064	
B^2	1263.81	1	1263.81	0.87	0.3933	
C^2	1321.84	1	1321.84	8.21	0.0352	
Residual	769.85	5	153.97	8.58	0.0326	
Lack of Fit	768.64	3	256.21	420.69	0.0024	significant
Pure Error	1.22	2	0.61			
Cor Total	7711.52	14				

R^2 = 0.9002 Adjusted R^2 = 0.7205 Predicted R^2 = −0.5951 Adeq Presion = 7.902.

Table 4. AY ANOVA results for response surface of quadratic model.

Source	Sum of Squares	df	Mean Square	F-Value	*p*-Value	
Model	3006.47	9	334.05			
A-Current intensity (A)	13.68	1	13.68	59.72	0.0001	significant
B-Time (min)	489.84	1	489.84	2.44	0.1787	
C-pH	14.42	1	14.42	87.57	0.0002	
AB	299.29	1	299.29	2.58	0.1693	
AC	1.00	1	1.00	53.51	0.0007	
BC	42.25	1	42.25	0.18	0.6900	
A^2	10.69	1	10.69	7.55	0.0404	
B^2	2041.10	1	2041.10	1.91	0.2254	
C^2	45.19	1	45.19	364.89	<0.0001	
Residual	27.97	5	5.59	8.08	0.0362	
Lack of Fit	20.62	3	6.87	1.87	0.3671	Not significant
Pure Error	7.35	2	3.68			
Cor Total	3034.43	14				

R^2 = 0.9908 Adjusted R^2 = 0.9742 Predicted R^2 = 0.8858 Adeq Presion = 24.309.

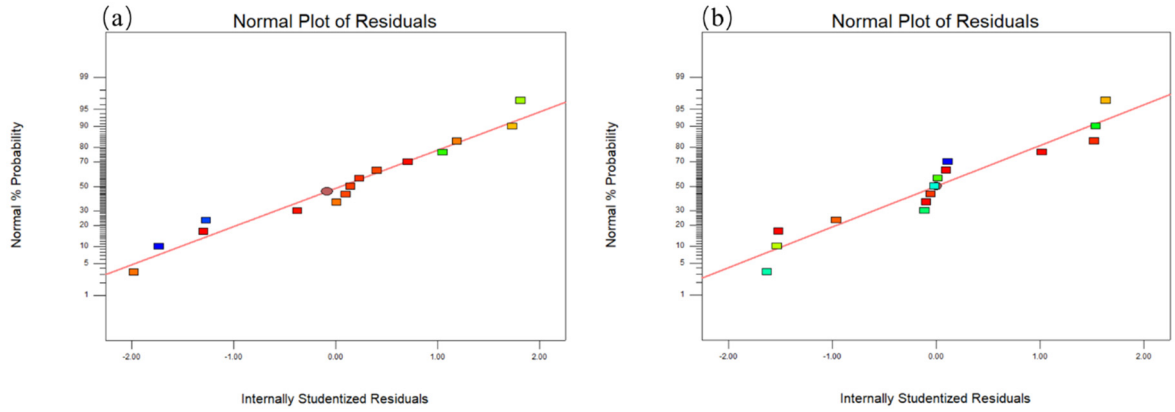

Figure 4. The Normal probability plot of studentized residuals of MO (**a**) and AY (**b**) of the model for the removal rates.

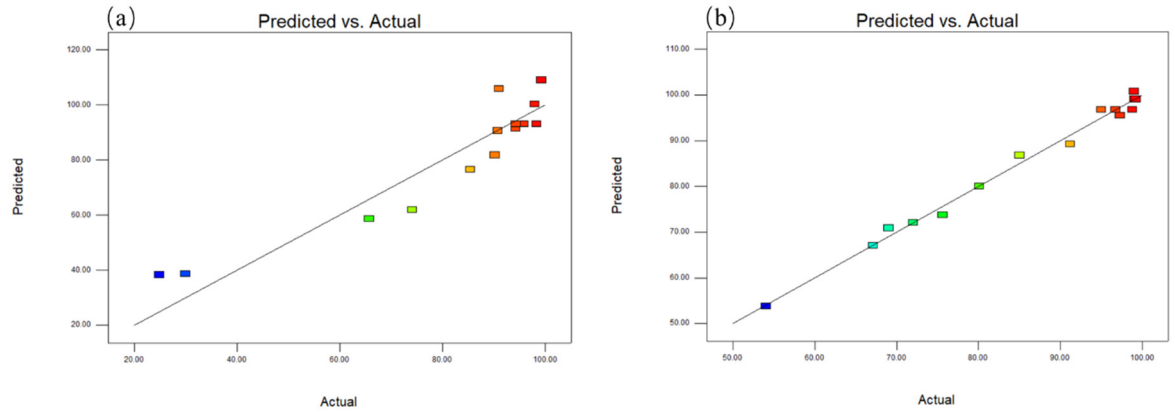

Figure 5. Experimental response values versus predicted response value of MO (**a**) and AY (**b**).

The RSM for the color removal rates according to the above three important parameters attained from the PREC experiments were depicted in Figure 6. Two parameters were demonstrated in 3D surface plots, while the other variable was kept at an optimum level ($\alpha = 0$). The interactions among the current intensity, time, and pH were corelated to the ANOVA results for the response surface of the quadratic model. In addition, when the color removal rate of MO and AY were predicted as 100% and 97.6%, correspondingly, the optimum conditions included the current intensity of 0.71 A and 0.57 A, the electrolysis time of 42.43 min and 31.08 min, and the pH values of 6.65 and 5.59. This conclusion demonstrates that the condition of PREC treatment for AY simulated wastewater was time-saving and energy conserving and, therefore, the azo dye of AY was more easily treated by the PREC technique than by MO. The regression model was a second-order response surface by the fitting analysis of multi-linear linear regression using software, as shown in the following formula (1 for MO) and (2 for AY).

$$Y = 93.18 + 1.61A + 23.59B + 2.04C - 0.025AB + 2.82AC + 1.85BC + 11.24A^2 - 20.54B^2 - 10.47C^2 \quad (1)$$

$$Y = 96.86 - 1.31A + 7.82B - 1.34C + 8.65AB - 0.50AC - 3.25BC - 1.70A^2 - 23.51B^2 + 3.5C^2 \quad (2)$$

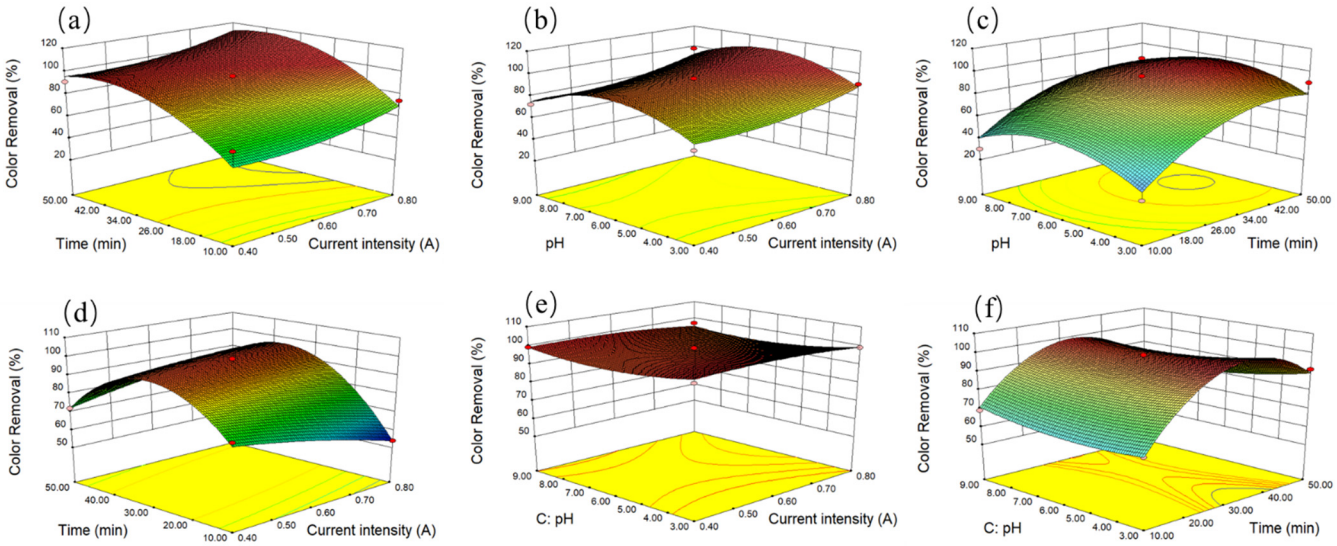

Figure 6. RSM for color removal rate of MO and AY as a function of current intensity and time (**a**,**d**), current density and pH (**b**,**e**), pH and time (**c**,**f**), respectively.

3.5. The Influence of Functional Groups

The degradation mechanism of MO and AY throughout the procedure of PREC process were also observed continually by the UV-Vis spectrophotometry analysis, when the optimum experimental conditions of the current intensity was 0.6 A, electrolyte was 2 g L^{-1} of NaCl, and the initial pH value was 6.0. The recorded UV spectra of MO and AY in the simulated aqueous solutions before and after the PREC treatment are illustrated in Figure 7. Overall, the MO and AY spectra in the visible region and the organics degradation in the UV region between 200 and 900 nm were investigated. The UV–Vis absorption spectrum of the initial MO solution (0 min) mainly covered two peaks at 248 nm and 462 nm, respectively. The peak at 462 nm could be ascribed to the π-π conjugated chain of the -N=N-, benzene ring structure, and the other one at 248 nm was the characteristic absorption band of the benzene ring [46]. On the other hand, the UV–Vis absorption spectrum of the original AY solution (0 min) contained two peaks at low wavelength of 240 nm and 376 nm, due to greater unsaturation than MO. The peak at 376 nm could be ascribed to the powerful π-π conjugated chain of the -N=N-, benzene ring structure, -NO_2, and -COO-, and the other one at 248 nm was the characteristic absorption band of the benzene ring. Clearly, different molecular structures resulted in the respective wavelength spectra of MO and AY.

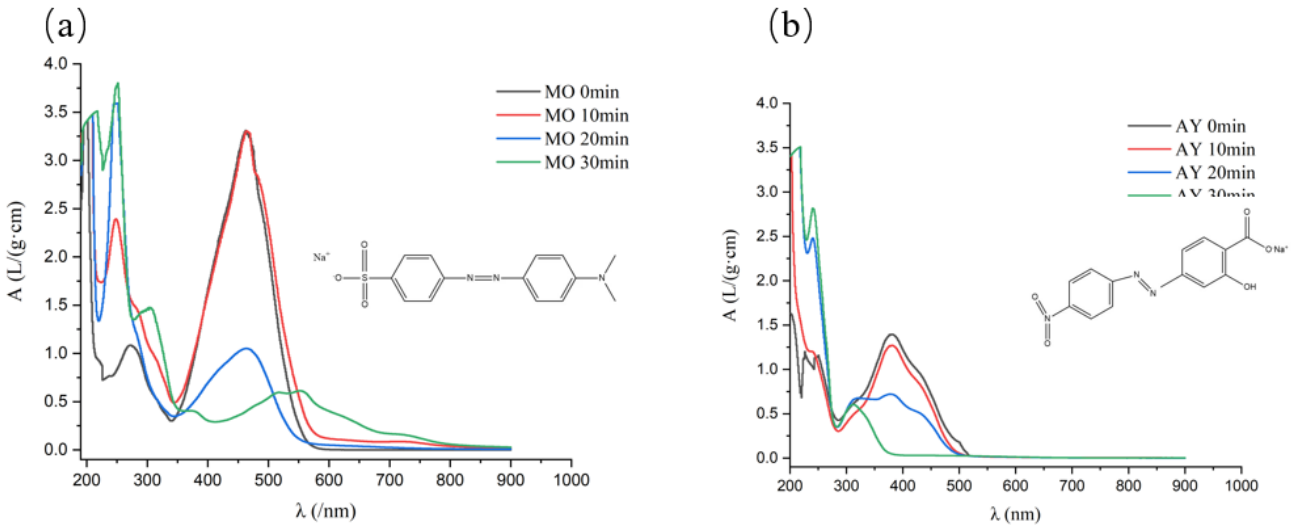

Figure 7. Absorbance spectra of MO (**a**) and AY (**b**) solution with the reaction time.

As depicted in Figure 7a, the wavelength at 463 nm of MO was diminished with the increase of the reaction time, due to the decrease in MO concentration that originated from flocculation. However, the respective wavelength at 248 nm of the benzene ring monomer was amplified gradually; this phenomenon demonstrated that the strong π-π conjugated system between the -N=N- bond that might be destroyed due to the oxidation reaction by ·OH and $O_2 \cdot^-$ in the PREC process. Within the initial 10 min, the absorbance at 463 nm was relative steady, while the COD removal rate still increased. This was likely because the adsorption on flocs was the main mechanism in the initial 10 min, with the oxidation-reduction then potentially taking effect in the subsequent process. As shown in the Figure 7b, the wavelength at 376 nm decreased gradually with the duration time, while the wavelength at 240 nm increased correspondingly and red shift slowly. It as well indicated that the -N=N- bond might be destroyed, and the new monomeric compound might be generated involving p-phenylenediamine and aminosalicylic acid. Moreover, the absorbance at 376 nm and COD was altogether weakened in the initial 10 min, which inferred that the adsorption on flocs and oxidation-reduction might come into effect simultaneously. This illustrates that the AY was propitious to promote the oxidation-reduction in the solution. Compared the functional group with MO, the strong electron-donating group of -OH in AY might be the reason for facilitating the reaction. Possibly this is because hydroxyl groups in AY would donate electrons to iron ions, or electrolyze out additional strong oxidizable substances such as hydroxyl free radicals, enhancing the degradation efficacy for such azo dyes [47]. The trend mentioned above was also consistent with the removal rates of COD for both MO and AY increasing within the first 20 min and then decreasing.

4. Conclusions

In summary, the degradation of MO and AY with different functional groups in the simulated wastewater with Fe-Fe electrodes by the PREC technique could be feasible. Intensive studies on simulated aqueous solutions containing MO or AY were implemented on the conditions of treatment involving the current intensity, pH, and electrolyte. The optimal removal rates for MO and AY could be achieved at 98.7% and 98.6% with Fe-Fe electrodes, when the current intensity and pH were set to 0.6 A and 6.0, respectively, and the electrolyte was selected as NaCl. An accurate predicted method of RSM was established to optimize the PREC process for the removal of MO and AY from simulated wastewater involving the above three influencing parameters. The reaction time was the main influence for both azo dyes, while the condition of PREC treatment for AY simulated wastewater was time-saving and energy conserving. Furthermore, comparing the temporal absorption variation in the absorbances of MO and AY throughout the procedure of PREC, the -N=N- bond was the breakout and the functional group of -OH in AY might play a vital role in the improvement of removal efficiency. As a result, the present study revealed that the excellent and efficient removal for color and COD, as well as the degradation of azo dyes could be achieved by the PREC. The RSM was a powerful tool for optimizing the operational parameters. The PREC technique could be a potential method to eliminate the contaminations of azo dyes with diverse functional groups from various wastewaters. In addition, extensive investigations about diverse electrolytes actuating on the electrode for the RSM analysis need to be implemented in our future studies.

Author Contributions: Conceptualization, Y.L. and J.B.; Data curation, C.L. and Y.L.; Formal analysis, C.L., W.Y. and L.S.; Funding acquisition, J.B.; Investigation, C.L. and X.W.; Methodology, Y.L. and J.B.; Project administration, Y.L. and J.B.; Resources, Y.L. and J.B.; Software, C.L. and L.S.; Supervision, Y.L., J.B. and X.W.; Validation, W.Y.; Visualization, L.S.; Writing—original draft, C.L. and Y.L.; Writing—review & editing, Y.L. and J.B. All authors have read and agreed to the published version of the manuscript.

Funding: This research was funded by the National Natural Science Foundation of China (No.21976124 and No.21507092), the Natural Science Foundation of Liaoning Province of China (No.2019-ZD-0217), and Liaoning Revitalization Talents Program (No.XLYC2007195).

Acknowledgments: Thanks for the financial supports from the National Natural Science Foundation of China (No.21976124 and No.21507092), the Natural Science Foundation of Liaoning Province of China (No.2019-ZD-0217), and Liaoning Revitalization Talents Program (No. XLYC2007195).

Conflicts of Interest: The authors declare no conflict of interest.

References

1. Pattnaik, P.; Dangayach, G.; Bhardwaj, A.K. A review on the sustainability of textile industries wastewater with and without treatment methodologies. *Rev. Environ. Health* **2018**, *33*, 163–203. [CrossRef] [PubMed]
2. Solis, M.; Solis, A.; Perez, H.I.; Manjarrez, N. Flores M Microbial decolouration of azo dyes: A review. *Process. Biochem.* **2012**, *47*, 1723–1748. [CrossRef]
3. Saratale, R.G.; Gandhi, S.S.; Purankar, M.V.; Kurade, M.; Govindwar, S.; Oh, S.E.; Saratale, G.D. Decolorization and detoxification of sulfonated azo dye C.I. Remazol Red and textile effluent by isolated Lysinibacillus sp. RGS. *J. Biosci. Bioeng.* **2013**, *115*, 658–667. [CrossRef]
4. Puvaneswari, N.; Muthukrishnan, J.; Gunasekaran, P. Toxicity assessment and microbial degradation of azo dyes. *Indian J. Exp. Boil.* **2006**, *44*, 618–626.
5. Ozturk, E.; Cinperi, N.C. Water efficiency and wastewater reduction in an integrated woolen textile mill. *J. Clean. Prod.* **2018**, *201*, 686–696. [CrossRef]
6. Hassan, M.M.; Carr, C.M. A critical review on recent advancements of the removal of reactive dyes from dyehouse effluent by ion-exchange adsorbents. *Chemosphere* **2018**, *209*, 201–219. [CrossRef]
7. Abe, F.R.; Soares, A.M.; de Oliveira, D.P.; Gravato, C.A. Toxicity of dyes to zebrafish at the biochemical level: Cellular energy allocation and neurotoxicity. *Environ. Pollut.* **2018**, *235*, 255–262. [CrossRef]
8. Du, C.F.; Xue, Y.T.; Wu, Z.S.; Wu, Z.L. Microwave-assisted one-step preparation of macadamia nut shell-based activated carbon for efficient adsorption of Reactive Blue. *New. J. Chem.* **2017**, *41*, 15373–15383. [CrossRef]
9. Kumar, P.S.; Sivaranjanee, R.; Vinothini, U.; Raghavi, M.; Rajasekar, K.; Ramakrishnan, K. Adsorption of dye onto raw and surface modified tamarind seeds: Isotherms, process design, kinetics and mechanism. *DESALINATION Water Treat.* **2014**, *52*, 2620–2633. [CrossRef]
10. Chung, K.-T. Azo dyes and human health: A review. *J. Environ. Sci. Health Part C* **2016**, *34*, 233–261. [CrossRef]
11. Saleh, T.; Gupta, V.K. Photo-catalyzed degradation of hazardous dye methyl orange by use of a composite catalyst consisting of multi-walled carbon nanotubes and titanium dioxide. *J. Colloid Interface Sci.* **2012**, *371*, 101–106. [CrossRef]
12. Chankhanittha, T.; Somaudon, V.; Watcharakitti, J.; Piyavarakorn, V.; Nanan, S. Performance of solvothermally grown Bi2MoO6 photocatalyst toward degradation of organic azo dyes and fluoroquinolone antibiotics. *Mater. Lett.* **2020**, *258*, 126764. [CrossRef]
13. Punzi, M.; Nilsson, F.; Anbalagan, A.; Svensson, B.-M.; Jönsson, K.; Mattiasson, B.; Jonstrup, M. Combined anaerobic–ozonation process for treatment of textile wastewater: Removal of acute toxicity and mutagenicity. *J. Hazard. Mater.* **2015**, *292*, 52–60. [CrossRef] [PubMed]
14. Subramaniam, R.; Ponnusamy, S.K. Novel adsorbent from agricultural waste (cashew NUT shell) for methylene blue dye removal: Optimization by response surface methodology. *Water Resour. Ind.* **2015**, *11*, 64–70. [CrossRef]
15. Bao, Y.; Niu, J.; Xu, Z.; Gao, D.; Shi, J.; Sun, X.; Huang, Q. Removal of perfluorooctane sulfonate (PFOS) and perfluorooctanoate (PFOA) from water by coagulation: Mechanisms and influencing factors. *J. Colloid Interface Sci.* **2014**, *434*, 59–64. [CrossRef] [PubMed]
16. Niu, J.; Li, Y.; Shang, E.; Xu, Z.; Liu, J. Electrochemical oxidation of perfluorinated compounds in water. *Chemosphere* **2016**, *146*, 526–538. [CrossRef]
17. Prajapati, A.K.; Chaudhari, P.K. Electrochemical treatment of rice grain-based distillery effluent: Chemical oxygen demand and colour removal. *Environ. Technol.* **2013**, *35*, 242–249. [CrossRef] [PubMed]
18. Stergiopoulos, D.; Dermentzis, K.; Giannakoudakis, P.; Sotiropoulos, S. Electrochemical decolorization and removal of indigo carmine textile dye from wastewater. *Glob. Nest. J.* **2014**, *16*, 499–506.
19. Cui, D.; Cui, M.-H.; Liang, B.; Liu, W.-Z.; Tang, Z.-E.; Wang, A.-J. Mutual effect between electrochemically active bacteria (EAB) and azo dye in bio-electrochemical system (BES). *Chemosphere* **2020**, *239*, 124787. [CrossRef]
20. Yavuz, Y.; Ögütveren, Ü.B. Treatment of industrial estate wastewater by the application of electrocoagulation process using iron electrodes. *J. Environ. Manag.* **2018**, *207*, 151–158. [CrossRef]
21. Shi, H.; Chiang, S.-Y.; Wang, Y.; Wang, Y.; Liang, S.; Zhou, J.; Fontanez, R.; Gao, S.; Huang, Q. An electrocoagulation and electrooxidation treatment train to remove and degrade per- and polyfluoroalkyl substances in aqueous solution. *Sci. Total. Environ.* **2021**, *788*, 147723. [CrossRef] [PubMed]
22. Khalifah, A.; Hayfaa, A.M.; Joseph, A.A.; Laith, A.A.; Rafid, A.K.; Mawada, A.; Abuduljaleel, A.J. Electrochemical removal of brilliant green dye from wastewater. In *IOP Conference Series: Materials Science and Engineering*; IOP Publishing: Bristol, UK, 2020; Volume 888, p. 012036.

23. Abdulhadi, B.A.; Kot, P.; Hashim, K.S.; Shaw, A.; Al Khaddar, R. Influence of current density and electrodes spacing on reactive red 120 dye removal from dyed water using electrocoagulation/electroflotation (EC/EF) process. In *IOP Conference Series: Materials Science and Engineering*; IOP Publishing: Bristol, UK, 2019; Volume 584, p. 012035. [CrossRef]
24. Núñez, J.; Yeber, M.; Cisternas, N.; Thibaut, R.; Medina, P.; Carrasco, C. Application of electrocoagulation for the efficient pollutants removal to reuse the treated wastewater in the dyeing process of the textile industry. *J. Hazard. Mater.* **2019**, *371*, 705–711. [CrossRef]
25. Bao, J.; Yu, W.-J.; Liu, Y.; Wang, X.; Liu, Z.-Q.; Duan, Y.-F. Removal of perfluoroalkanesulfonic acids (PFSAs) from synthetic and natural groundwater by electrocoagulation. *Chemosphere* **2020**, *248*, 125951. [CrossRef]
26. Liu, Y.; Hu, X.-M.; Zhao, Y.; Wang, J.; Lu, M.-X.; Peng, F.-H.; Bao, J. Removal of perfluorooctanoic acid in simulated and natural waters with different electrode materials by electrocoagulation. *Chemosphere* **2018**, *201*, 303–309. [CrossRef]
27. Pi, K.W.; Xiao, Q.; Zhang, H.Q.; Xia, M.; Gerson, A.R. Decolorization of synthetic Methyl Orange wastewater by electrocoagulation with periodic reversal of electrodes and optimization by RSM. *Process. Saf. Environ. Prot.* **2014**, *92*, 796–806. [CrossRef]
28. Oliveira, M.T.; Garcia, L.F.; Siqueira, A.C.R.; Somerset, V.; Gil, E.S. Electrocoagulation of the indigo carmine dye using electrodes produced from the compression of metallurgical filing wastes. *Int. J. Environ Sci. Technol.* **2019**, *17*, 1657–1662. [CrossRef]
29. Gautam, K.; Kamsonlian, S.; Kumar, S. Removal of Reactive Red 120 dye from wastewater using electrocoagulation: Optimization using multivariate approach, economic analysis, and sludge characterization. *Sep. Sci. Technol.* **2019**, *55*, 3412–3426. [CrossRef]
30. Hashim, K.S.; Shaw, A.; Al Khaddar, R.; Pedrola, M.O.; Phipps, D. Iron removal, energy consumption and operating cost of electrocoagulation of drinking water using a new flow column reactor. *J. Environ. Manag.* **2017**, *189*, 98–108. [CrossRef]
31. Karamati-Niaragh, E.; Moghaddam, M.R.A.; Emamjomeh, M.M.; Nazlabadi, E. Evaluation of direct and alternating current on nitrate removal using a continuous electrocoagulation process: Economical and environmental approaches through RSM. *J. Environ. Manag.* **2019**, *230*, 245–254. [CrossRef]
32. Abbasi, S.; Mirghorayshi, M.; Zinadini, S.; Zinatizadeh, A. A novel single continuous electrocoagulation process for treatment of licorice processing wastewater: Optimization of operating factors using RSM. *Process Saf. Environ. Prot.* **2020**, *134*, 323–332. [CrossRef]
33. Bhatti, M.S.; Kapoor, D.; Kalia, R.K.; Reddy, A.S.; Thukral, A.K. RSM and ANN modeling for electrocoagulation of copper from simulated wastewater: Multi objective optimization using genetic algorithm approach. *Desalination* **2011**, *274*, 74–80. [CrossRef]
34. Verma, A.K. Treatment of textile wastewaters by electrocoagulation employing Fe-Al composite electrode. *J. Water Process. Eng.* **2017**, *20*, 168–172. [CrossRef]
35. Irki, S.; Ghernaout, D.; Naceur, M.W. Decolourization of Methyl Orange (MO) by electrocoagulation (EC) using iron electrodes under a magnetic field (MF). *DESALINATION Water Treat.* **2017**, *79*, 368–377. [CrossRef]
36. Tahreen, A.; Jami, M.S.; Ali, F. Role of electrocoagulation in wastewater treatment: A developmental review. *J. Water Process Eng.* **2020**, *37*, 101440. [CrossRef]
37. Brahmi, K.; Bouguerra, W.; Hamrouni, B.; Elaloui, E.; Loungou, M.; Tlili, Z. Investigation of electrocoagulation reactor design parameters effect on the removal of cadmium from synthetic and phosphate industrial wastewater. *Arab. J. Chem.* **2019**, *12*, 1848–1859.
38. Devlin, T.R.; Kowalski, M.S.; Pagaduan, E.; Zhang, X.; Wei, V.; Oleszkiewicz, J.A. Electrocoagulation of wastewater using aluminum, iron, and magnesium electrodes. *J. Hazard. Mater.* **2019**, *368*, 862–868. [CrossRef] [PubMed]
39. Qian, A.; Yuan, S.; Xie, S.; Tong, M.; Zhang, P.; Zheng, Y. Oxidizing Capacity of Iron Electrocoagulation Systems for Refractory Organic Contaminant Transformation. *Environ. Sci. Technol.* **2019**, *53*, 12629–12638. [CrossRef] [PubMed]
40. Mollah, M.Y.A.; Gomes, J.A.; Das, K.K.; Cocke, D.L. Electrochemical treatment of Orange II dye solution—Use of aluminum sacrificial electrodes and floc characterization. *J. Hazard. Mater.* **2010**, *174*, 851–858. [CrossRef] [PubMed]
41. Naje, A.S.; Chelliapan, S.; Zakaria, Z.; Ajeel, M.A.; Alaba, P.A. A review of electrocoagulation technology for the treatment of textile wastewater. *Rev. Chem. Eng.* **2017**, *33*, 263–292. [CrossRef]
42. Ingelsson, M.; Yasri, N.; Roberts, E.P. Electrode passivation, faradaic efficiency, and performance enhancement strategies in electrocoagulation—a review. *Water Res.* **2020**, *187*, 116433. [CrossRef]
43. Garcia-Segura, S.; Eiband, M.M.S.G.; Melo, J.V.; Martínez-Huitlea, C.A. Electrocoagulation and advanced electrocoagulation processes: A general review about the fundamentals, emerging applications and its association with other technologies. *J. Electroanal. Chem.* **2017**, *801*, 267–299. [CrossRef]
44. Hakizimana, J.N.; Gourich, B.; Chafi, M.; Stiriba, Y.; Vial, C. Electrocoagulation process in water treatment: A review of electrocoagulation modeling approaches. *Desalination* **2017**, *404*, 1–21. [CrossRef]
45. Wu, Z.; Dong, J.; Yao, Y.; Yang, Y.; Wei, F. Continuous flowing electrocoagulation reactor for efficient removal of azo dyes: Kinetic and isotherm studies of adsorption. *Environ. Technol. Innov.* **2021**, *22*, 101448. [CrossRef]
46. Nisha, S.K.; Sivakumar, S.; Achutha, S. Polyvinyl alcohol/methyl orange flexible film as reusable pH indicator. *Mater. Today Proc.* **2021**, *42*, 1008–1011. [CrossRef]
47. Kong, X.W. *Organic Chemistry*, 2nd ed.; Chemical Industry Press: Beijing, China, 2020; pp. 73–74. (In Chinese)